70

SATELLITE & MESOMETEOROLOGY RESEARCH PROJECT

Department of the Geophysical Sciences
The University of Chicago

COMPUTATION OF HEIGHT AND VELOCITY OF CLOUDS FROM DUAL, WHOLE-SKY, TIME-LAPSE PICTURE SEQUENCES

by

Dorothy L. Bradbury and Tetsuya Fujita
The University of Chicago

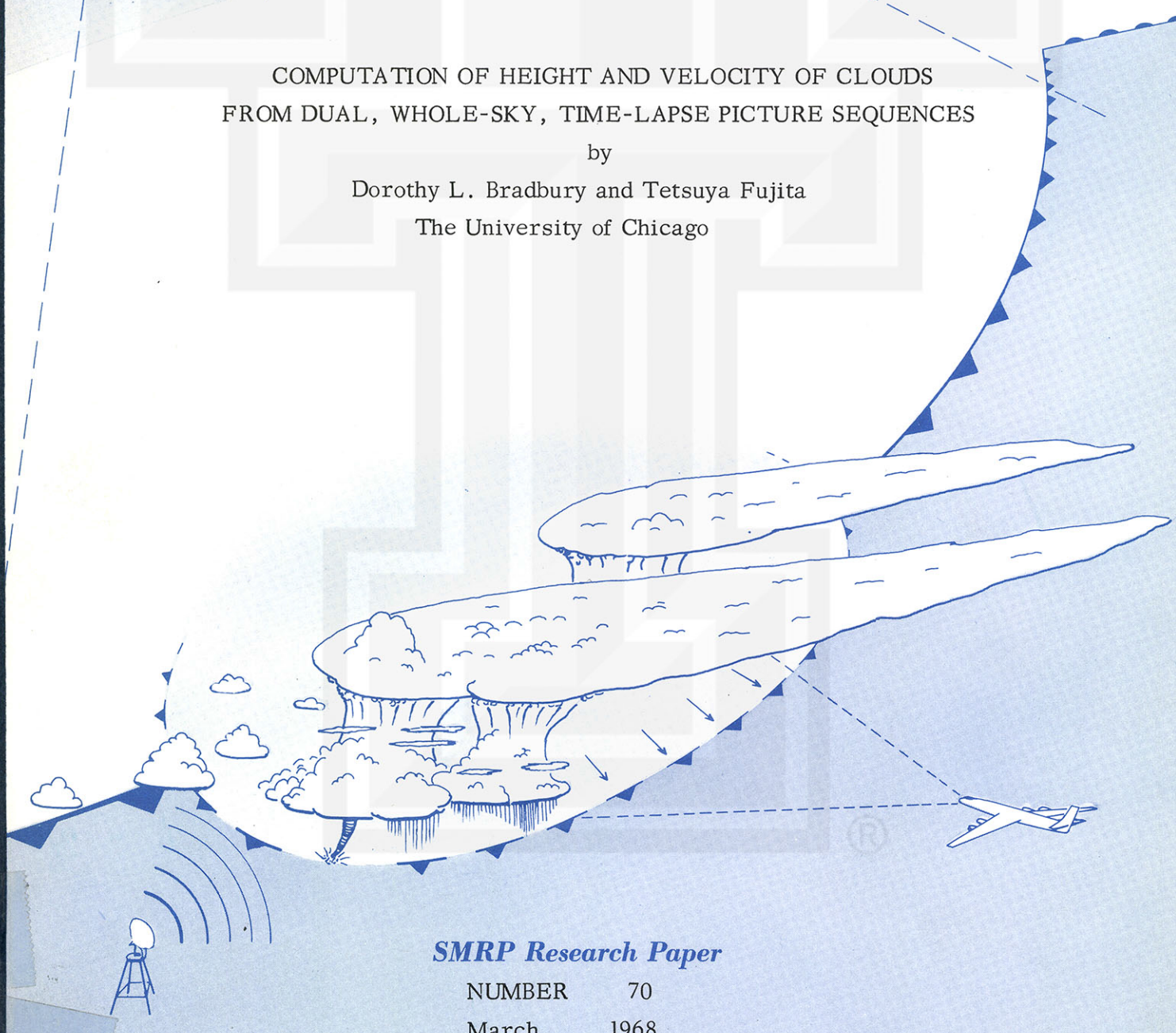

SMRP Research Paper
NUMBER 70
March 1968

MESOMETEOROLOGY PROJECT --- RESEARCH PAPERS

1.* Report on the Chicago Tornado of March 4, 1961 - Rodger A. Brown and Tetsuya Fujita

2.* Index to the NSSP Surface Network - Tetsuya Fujita

3.* Outline of a Technique for Precise Rectification of Satellite Cloud Photographs - Tetsuya Fujita

4.* Horizontal Structure of Mountain Winds - Henry A. Brown

5.* An Investigation of Developmental Processes of the Wake Depression Through Excess Pressure Analysis of Nocturnal Showers - Joseph L. Goldman

6.* Precipitation in the 1960 Flagstaff Mesometeorological Network - Kenneth A. Styber

7.** On a Method of Single- and Dual-Image Photogrammetry of Panoramic Aerial Photographs - Tetsuya Fujita

8. A Review of Researches on Analytical Mesometeorology - Tetsuya Fujita

9.* Meteorological Interpretations of Convective Nephsystems Appearing in TIROS Cloud Photographs - Tetsuya Fujita, Toshimitsu Ushijima, William A. Hass, and George T. Dellert, Jr.

10.* Study of the Development of Prefrontal Squall-Systems Using NSSP Network Data - Joseph L. Goldman

11. Analysis of Selected Aircraft Data from NSSP Operation, 1962 - Tetsuya Fujita

12. Study of a Long Condensation Trail Photographed by TIROS I - Toshimitsu Ushijima

13. A Technique for Precise Analysis of Satellite Data; Volume I - Photogrammetry (Published as MSL Report No. 14) - Tetsuya Fujita

14. Investigation of a Summer Jet Stream Using TIROS and Aerological Data - Kozo Ninomiya

15. Outline of a Theory and Examples for Precise Analysis of Satellite Radiation Data - Tetsuya Fujita

16. Preliminary Result of Analysis of the Cumulonimbus Cloud of April 21, 1961 - Tetsuya Fujita and James Arnold

17. A Technique for Precise Analysis of Satellite Photographs - Tetsuya Fujita

18.* Evaluation of Limb Darkening from TIROS III Radiation Data - S.H.H. Larsen, Tetsuya Fujita, and W.L. Fletcher

19. Synoptic Interpretation of TIROS III Measurements of Infrared Radiation - Finn Pedersen and Tetsuya Fujita

20.* TIROS III Measurements of Terrestrial Radiation and Reflected and Scattered Solar Radiation - S.H.H. Larsen, Tetsuya Fujita, and W.L. Fletcher

21. On the Low-level Structure of a Squall Line - Henry A. Brown

22.* Thunderstorms and the Low-level Jet - William D. Bonner

23.* The Mesoanalysis of an Organized Convective System - Henry A. Brown

24. Preliminary Radar and Photogrammetric Study of the Illinois Tornadoes of April 17 and 22, 1963 - Joseph L. Goldman and Tetsuya Fujita

25. Use of TIROS Pictures for Studies of the Internal Structure of Tropical Storms - Tetsuya Fujita with Rectified Pictures from TIROS I Orbit 125, R/O 128 - Toshimitsu Ushijima

26. An Experiment in the Determination of Geostrophic and Isallobaric Winds from NSSP Pressure Data - William Bonner

27. Proposed Mechanism of Hook Echo Formation - Tetsuya Fujita with a Preliminary Mesosynoptic Analysis of Tornado Cyclone Case of May 26, 1963 - Tetsuya Fujita and Robbi Stuhmer

28. The Decaying Stage of Hurricane Anna of July 1961 as Portrayed by TIROS Cloud Photographs and Infrared Radiation from the Top of the Storm - Tetsuya Fujita and James Arnold

29. A Technique for Precise Analysis of Satellite Data, Volume II - Radiation Analysis, Section 6. Fixed-Position Scanning - Tetsuya Fujita

30. Evaluation of Errors in the Graphical Rectification of Satellite Photographs - Tetsuya Fujita

31. Tables of Scan Nadir and Horizontal Angles - William D. Bonner

32. A Simplified Grid Technique for Determining Scan Lines Generated by the TIROS Scanning Radiometer - James E. Arnold

33. A Study of Cumulus Clouds over the Flagstaff Research Network with the Use of U-2 Photographs - Dorothy L. Bradbury and Tetsuya Fujita

34. The Scanning Printer and Its Application to Detailed Analysis of Satellite Radiation Data - Tetsuya Fujita

35. Synoptic Study of Cold Air Outbreak over the Mediterranean using Satellite Photographs and Radiation Data - Aasmund Rabbe and Tetsuya Fujita

36. Accurate Calibration of Doppler Winds for their use in the Computation of Mesoscale Wind Fields - Tetsuya Fujita

37. Proposed Operation of Intrumented Aircraft for Research on Moisture Fronts and Wake Depressions - Tetsuya Fujita and Dorothy L. Bradbury

38. Statistical and Kinematical Properties of the Low-level Jet Stream - William D. Bonner

39. The Illinois Tornadoes of 17 and 22 April 1963 - Joseph L. Goldman

40. Resolution of the Nimbus High Resolution Infrared Radiometer - Tetsuya Fujita and William R. Bandeen

41. On the Determination of the Exchange Coefficients in Convective Clouds - Rodger A. Brown

* Out of Print
** To be published

(Continued on back cover)

SATELLITE AND MESOMETEOROLOGY RESEARCH PROJECT
Department of the Geophysical Sciences
The University of Chicago

COMPUTATION OF HEIGHT AND VELOCITY OF CLOUDS FROM DUAL, WHOLE-SKY, TIME-LAPSE PICTURE SEQUENCES

by
Dorothy L. Bradbury and Tetsuya Fujita
The University of Chicago

SMRP Research Paper No. 70

March 1968

The research reported in this paper has been sponsored by the Meteorological Satellite Laboratory, ESSA, under Grant Cwb WBG-34 and the National Science Foundation under Grant No. GA-864.

COMPUTATION OF HEIGHT AND VELOCITY OF CLOUDS FROM DUAL, WHOLE-SKY, TIME-LAPSE PICTURE SEQUENCES[1]

by

Dorothy L. Bradbury and Tetsuya Fujita

The University of Chicago

1. Introduction

The Satellite and Mesometeorology Research Project of the University of Chicago together with St. Louis University established a camera network of stations atop the northern rim of Haleakala on the island of Maui during the early part of March 1967. The network was in operation from 13 March through 3 April 1967. The purpose of the network was to gather photographic cloud data during the period of the Line Island Experiment and the ATS-I picture acquisition in order to study the time changes in mesoscale nephsystems and to compute heights and motions of clouds in the region of the Hawaiian islands.

One of the camera systems used to gather cloud data was the whole-sky system designed and manufactured by Meteorology Research, Inc. of Altadena, California. It is the purpose of this paper to describe the technique used for calibrating the whole-sky mirror and then to compute the cloud height and motions from time-lapse movies taken with the whole-sky cameras.

2. SMRP Camera Network of Haleakala, Maui

Figure 1 shows the photographic network established on the northern rim of Haleakala. Three different camera systems were used to gather photographic cloud data from the Hawaiian area. They were two stationary wide-angle movie cameras, two panoramic cameras, and two whole-sky cameras. The two wide-angle time-lapse cameras were mounted on the roof of a building at the Kolekole site at an elevation of around 9990 ft. with one camera pointing toward the island

---

[1] The research reported in this paper has been sponsored by the Meteorological Satellite Laboratory, ESSA, under Grant Cwb WBG-34 and the National Science Foundation under Grant No. GA-864.

of Hawaii and the other toward Lanai. These cameras were set to take 16 mm color movies at 15-sec intervals during the daylight hours. At the Red Hill site (elevation 10,010 ft), a whole-sky system and a panoramic camera stand were erected about 25 ft apart and this site was designated station "A". The whole sky cameras were set to take 16-mm color movies at 20-sec intervals during the daylight hours. For the panoramic views, 35-mm cameras were manually operated using infrared film. Eight pictures were taken, one centered on each octant beginning with N, NE, etc., every 20 min and as near as possible to the time of the ATS picture acquisition schedule. The second whole-sky station ("B") was established at the Kalahaku site (elevation 9320 ft), a distance of 3.6 km north-northeast of station "A". In order to get the best possible view in all octants, the panoramic camera stand was placed on a peak (elevation 9410 ft) approximately 0.3 km south-southwest of the whole-sky site.

Figure 2 shows a close-up of the parabolic mirror and data table of the model A-20-EW whole-sky camera system. Time in hours, minutes, and seconds is read directly from the face of the Accutron clock mounted on a pedestal at the center of the mirror. A counter, barely visible in this picture, records the number of elapsed days. The wind direction vane is mounted on a stand directly above the center of the mirror and thus the wind direction can be determined from the whole sky picture. Air temperature and relative humidity are indicated on the dials inset in the data table. A tipping bucket rain gauge drives a set of counters to record rainfall amounts in hundredths of an inch (upper set of counters). The cumulative wind run measured in sixtieths of a statute mile is indicated in the lower set of counters in Fig. 2. These counters are driven by a cup anemometer mounted on a short tower placed a short distance from the whole-sky data table.

A 100-ft roll of 16 mm film was adequate for operating one day with the camera set to take pictures at 20-sec intervals. The camera systems were serviced and film changed as near as possible to sunrise in order that the cloud photography not be interrupted during the middle of the day.

3. Calibration of Whole-Sky View Using Solar Image

Before cloud heights and motions can be computed from the whole-sky cloud pictures the parabolic mirrors must first be calibrated to determine the horizon (apparent),

zero azimuth, and solar zenith angles or cloud elevation angles. One method of doing this would be to compute the angles theoretically by using the dimensions of the parabolic mirror. This method assumes that the mirrors are perfect and identical and that the principal point was exactly at the center of the circular image. It was found, however, that the more practical method would be to calibrate each mirror individually by tracing the path of the subsolar point on the whole sky picture from sunrise to sunset on a nearly cloudless day. Figure 3 shows an example of such a tracing made for 14 March 1967 for a camera located on Maui at an elevation of approximately 10,000 feet. The camera site was at 20 deg 42 min 50 sec N 156 deg 15 min 23 sec W. When the sun is at very low elevation angles, near sunrise and sunset, the exact center of its image is difficult to locate. In most cases the horizon (zero elevation) can be readily identified on the picture and the solar image track can be extended to intersect the apparent horizon.

The horizon can also be located by using the panoramic IR pictures which, in our case, were taken simultaneously with the whole sky pictures. On these, the horizon is very marked and by matching cloud elements, topography, etc., on the two different types of pictures a reliable apparent horizon can be drawn.

If the optical axis of the camera and that of the mirror are identical, the center of the circular image and the principal point of the mirror will coincide and the apparent horizon and outer boundary of the circular image will be concentric circles. In this case (Fig. 3) there is a slight shift of the principal point to the right of the center of the circular image. This resulted in minor complications in determining the correct zero azimuth. If the center of the image and the principal point of the mirror coincide, the perpendicular bisector of the chord joining the two ends of the subpoint track would pass through the principal point, intersect the subpoint track at local noon, and point toward the north (zero azimuth). In our case, it was necessary to first locate local noon for the whole-sky camera station (122502 HST) on the subpoint track. This can be interpolated from the picture times taken several minutes on both sides of noonday. A perpendicular erected at this point will point to zero azimuth. From this the remaining azimuth angles are readily determined.

The method used to determine the geodetic latitude and longitude of the subsolar point was that proposed by Fujita (1963) in describing the photogrammetric technique

of precise analysis of satellite data. Celestial coordinates permit us to express the motion of a satellite (in this case the sun) with respect to a coordinate system which does not rotate as the earth does. Since the rotation rate of the earth's ascending node is negligible for the time intervals we are interested in, it is convenient to use the celestial coordinates associated with a celestial sphere with its center at the center of the earth. The coordinates are geocentric distances, declination, and right ascension. Since the geocentric distance of the sun is so great, the declination of the sun is equal to the geodetic latitude of the subsolar point or solar image on the whole sky picture. The geodetic latitude and longitude of the subsolar point can be determined by using Tables XIV and XV which were computed by Fujita (1963) and include values up through the year 1970. Picture time is first converted to Greenwich Meridian Time before using the tables.

As an example we will compute the geodetic latitude and longitude for the subsolar point on the picture taken at 210532 GMT (110532 HST) on 14 March 1967 from camera station "A".

Computation of ϕ^* , Geodetic Latitude of Subsolar Point, from Table XIV

Day function	-2.8
Year and hour function	0.3
	-2.5

Computation of θ^*, Geodetic Longitude of Subsolar Point, from Table XV

Day function	+2.3	
Hour function	-135.0	
Minute function	-1.4	
	-134.1	+360.0 = 225.9

The geodetic latitude and longitude of each selected point along the solar path was computed in this manner.

The next step is to convert these values into solar zenith angles. This was done by using the transverse equidistant cylindrical projection chart (TEC) and its overlay.

Figure 4 shows a section of the TEC chart and the TEC overlay which were designed by Fujita (1963). The location of the camera station is plotted on the TEC chart as near as possible to the central meridian of the chart and the meridians are then labeled in terms of right ascension from Greenwich. For example, the longitude of Station "A" is 156 deg 15 min 23 sec W which when converted to right ascention would be 203 deg 44 min 37 sec E. Thus the central meridian on the TEC chart is labeled 205 and the other meridians labeled accordingly, with increasing values to the right and decreasing to the left as shown in Fig. 4. The zero declination or geodetic latitude represents the equator, and positive declination values are in the northern hemisphere and negative values in the southern hemisphere. The computed values of geodetic latitude and longitude for the subsolar points are plotted on the TEC chart.

Next, the TEC overlay is placed over the TEC chart with the pole coinciding with the camera station and the principal meridian intersecting the subsolar point track at local noontime (azimuth 180°). The zenith angle, ζ , of each subsolar point is read directly from the latitude circles on the overlay and the azimuth from the meridians. These zenith angle values are then plotted on the subsolar track on the whole sky image and concentric circles with the center at the principal point are drawn at 10 degree intervals or whatever interval is desired as shown in Fig. 5. For convenience in computing cloud motions these are relabeled to elevation angles, (90 - ζ). Such an overlay grid can now be superimposed upon any of the whole-sky pictures and the elevation angle of all clouds and cloud elements read directly.

An alternative method of computing both the zenith angle and azimuth of the sun as a function of the locations of the subsolar point and the camera station is to solve a spherical triangle on the earth. Keeping in mind that the solar zenith angle is equal to the geocentric angle between the station and the subsolar point, we write

$$\cos\zeta^* = \sin\phi \sin\phi^* + \cos\phi \cos\phi^* \cos(\theta^* - \theta) \qquad (1)$$

where the superscript * denoted the sun; ϕ , the latitude; θ , the longitude; and ζ , the zenith angle.

After computing the solar zenith angle, ζ^* , we apply the sine law to the spherical triangle formed by the camera station, the subsolar point, and the terrestrial north pole, thus

$$\sin \alpha = \frac{\cos \phi^* \sin(\theta^* - \theta)}{\sin \zeta^*} \qquad (2)$$

where α^* denotes the azimuth of the sun as viewed from the camera station. It should be noted that both ϕ^* and θ^* must be given as a function of time if one is computing successive positions of the sun.

4. Selection of Proper Stereo-Pairs

The two whole-sky camera systems were set to take pictures as near synchronous as possible and at about twenty-second intervals. The timing mechanism was very sensitive to temperature changes and because of this there were some slight variations in time-lapse intervals.

In order to do accurate triangulation it is essential that the pair of stereo pictures be very near to synchronous. To select such a pair of pictures, the following procedure was employed. For the day in question, 15 March 1967 in this case, the film from each of the two cameras was projected, with the frame counter set at 1 for the first frame, and the frame number and picture time tabulated for a period of about 10 minutes near a specified time of day for which computations were to be made. Figure 6 shows the plot of frame number vs. local time for each of the two whole-sky cameras. As can be seen the picture intervals were not identical and that during a 10-min period there were two periods, one consisting of 4 frames (4 stereo-pairs) and the other of 3 frames (3 stereo-pairs) when the two pictures were taken within two seconds of one another. For all practical purposes this short time difference is acceptable. If more precise measurements are required for computing cloud motion, etc., linear interpolation can be used to have the two cloud elements exactly synchronous.

5. Determination of Displacement of Selected Cloud Elements on Whole-Sky Images

After choosing suitable pairs of whole-sky pictures, working-size prints are made from these frames. One next selects clouds or cloud elements that appear on these consecutive pictures for three or four frames, or more, from the two sequences of pictures. It is essential that the same cloud be identified on both pictures of a stereo-

pair. Figure 7 shows a stereo-pair of pictures with six clouds and cloud elements identified on both pictures. The length of time that a cloud or cloud element can be tracked will depend upon the stage of development at the initial frame, its rate of motion, and the complexity of the sky cover. If the cloud is in its developing stage it is likely that it can be followed over a longer period than if it were in its dissipating stage. If the clouds are moving at a very rapid rate they will probably be out of range of one or the other cameras witnin a short time. When clouds at two or more levels are present, the lower level clouds may obscure a cloud element at a higher level from one of the pictures.

The relative displacement of the selected clouds can be determined by placing an overlay sheet on the first picture of the series, plotting the position of each cloud element which is identified by an assigned number, and then doing the same for the final picture of the series. Lines joining the two points with identical numbers represents the relative displacement during the time interval.

6. Triangulation of Cloud Positions and Velocity Computations

On a sheet of tracing paper the two camera stations are plotted with the baseline between them drawn to scale. After superimposing one at a time, the camera station point over the principal point of the whole sky picture the azimuth rays are drawn from the station through each cloud element. These lines should be labeled by a number to match with the cloud number. The intersection of a pair of identically numbered rays represents the position of the cloud element and its distance from the camera station can be determined by direct measurement. Figure 8 shows six such sets of azimuth rays for the six from a large number of clouds on a pair of pictures shown in Fig. 7.

Using the same technique on a pair of pictures three of four frames later the distances of as many as possible of the same cloud elements from the camera stations are determined. The displacement of these cloud elements can be determined by direct measurement and converted into cloud motion expressed in direction and knots. It can be assumed that in this short interval of time that the cloud height remains constant.

Table I lists the computed distance from each camera station of 28 cloud elements selected from a stereo-apir of pictures and the average cloud motion for 10 of these

clouds. It was not possible to identify all of the same 28 clouds in a sequence of three or four frames. The mean cloud motion values recorded represent the average values computed from the two camera stations.

7. Computation of Cloud Heights

Using the elevation angle grid described in section 3 the elevation angle of each cloud element is tabulated for each camera station. The height of the cloud element above sea level is determined from

$$h = h_0 + D \tan \alpha \qquad (3)$$

where D is the horizontal distance of the cloud from the station; h, the cloud height above station elevation; h_0 , the station elevation; and α , the elevation angle.

Listed in Table I are the computed cloud heights from each camera station for the 28 cloud elements in the first pair of stereo-pictures of the series. As can be seen the two values agree quite well; the average difference between values for the 28 cases was 0.1 km. This is well within the range of expected accuracy since it is difficult to read elevation angles of the cloud elements to an accuracy of less than 1 degree.

8. Summary and Conclusions

When used as a stereo-pair, whole-sky cloud pictures can be very useful for studying cloud motions and heights. But it is essential that an image from each of the cameras be accurately calibrated if one is to have reliable results from computations made from such pictures. It was found that a very accurate method of calibration was to use the subsolar point track on the whole-sky image. From this the azimuth and elevation angles for cloud positions can be determined.

In this study the cameras were operated at an elevation between 9000 and 10,000 feet and were used to study clouds in the vicinity of the Hawaiian islands. Such whole-sky pictures could be equally useful for studying cloud motion and growth in any area in the tropics and at any elevation.

From the experience gained from our use of the whole-sky pictures taken by the MRI Model A-20-EW several suggestions can be made to future users of the cameras.

Table I. Computed range of clouds from whole-sky camera stations, their height (MSL) and cloud motion for clouds shown in the stereo-pair in Fig. 7. Cloud motion was computed as a 1-min average. Clouds numbered 1 to 6 are shown in Fig. 7.

Cloud No.	Distance from A (km)	Distance from B (km)	Elev. ∠ A (deg)	Elev. ∠ B (deg)	Height A (km)	Height B (km)	Mean Cloud Motion (kt)
1	17.0	13.5	8.5	11.0	5.5	5.5	
2	7.1	5.0	21.0	30.0	5.7	5.7	
3	7.1	6.6	19.0	20.0	5.4	5.3	31.9
4	5.1	6.6	24.0	19.4	5.2	5.2	38.4
5	5.9	9.1	27.2	17.0	5.9	5.7	45.3
6	8.4	7.7	19.5	24.4	6.0	6.3	57.4
7	11.3	8.2	10.0	15.0	5.0	5.0	
8	11.4	8.8	12.0	16.3	5.4	5.4	
9	7.4	5.1	18.0	25.0	5.4	5.2	
10	9.9	7.8	8.5	11.0	4.5	4.4	
11	10.0	8.4	7.5	10.7	4.3	4.4	
12	9.6	8.1	7.2	11.2	4.2	4.4	
13	6.6	5.3	20.0	25.3	5.4	5.3	
14	5.0	4.7	28.0	29.7	5.6	5.5	
15	3.6	4.7	34.3	29.0	5.5	5.5	
16	7.4	7.9	16.8	16.5	5.2	5.2	33.5
17	7.8	8.9	17.0	13.7	5.3	5.0	39.9
18	10.3	11.5	11.3	11.0	5.1	5.1	39.9
19	7.3	9.0	18.0	15.0	5.4	5.2	
20	4.0	6.4	29.5	20.0	5.3	5.2	
21	3.4	6.2	29.8	20.0	5.0	5.1	31.9
22	5.9	8.3	20.0	15.2	5.2	5.1	
23	6.8	10.0	13.5	10.2	4.7	4.7	31.9
24	3.6	7.1	20.0	13.0	4.3	4.5	
25	2.2	5.6	39.0	20.0	4.8	4.9	
26	22.3	22.2	10.0	10.0	6.9	6.8	
27	5.4	5.8	25.4	27.8	5.6	5.9	50.0
28	8.0	9.2	20.0	19.0	5.9	5.9	

Because the clock is mounted in the center of the mirror much of the area near the celestial zenith is obscured and cloud motion and height computations made by using elevation angles greater than 60 degrees were not tried. This is not necessarily a weakness of the camera system since it is difficult to track cloud elements that pass directly over the stations as they are observed from below by one camera and from an angle by the other. In a like manner, those clouds with very low elevation angles are generally difficult to identify in a series of pictures. It was found that best results were obtained from using cloud elements at elevation angles between 15 and 60 degrees. It is not possible to determine by triangulation the range of clouds with azimuth angles coinciding with or very close to that of the base line between the two camera stations.

Errors in computations of cloud motion and height may be due to one or more of the following conditions, provided the whole-sky images have been accurately calibrated.

1. On consecutive frames the identifying mark placed on the cloud or cloud element may not be in exactly the same area of the cloud due to different optical angles of view.

2. The cloud element may be moving rapidly toward the camera station and thus increase in size very rapidly between frames. The exact area of the cloud is difficult to match in two vastly different sizes of cloud.

3. Change in the shape and size of the cloud between frames causes displacement of the specific area or identifying feature of the cloud being followed.

Acknowledgments

The field operations and research reported in this paper was sponsored by the National Science Foundation under Grant No. GA-864 and the Environmental Science Services Administration (ESSA) under grant Cwb WBG-34. The two whole-sky cameras, Model A-20-EW, were loaned to the National Science Foundation by the Desert Flight Center, Fort Douglas, Utah.

Meteorology Research, Inc., Altadena, California, transported the cameras to the site and returned them to Fort Douglas at the end of the field operation period. The cameras were serviced and maintained by Mr. William Carlson, field engineer for MRI and the authors are grateful to him for his excellent cooperation and assistance. Much credit for the success of the field operations is due Mr. Arthur Z. Loesch for his dedicated assistance in setting up the camera stations and participating in their operation and maintenance.

REFERENCES

Fujita, T., 1963: A Technique for Precise Analysis for Satellite Data; Volume I - Photogrammetry, U.S. Weather Bureau, Meteorological Satellite Laboratory, Report No. 14, 106 pp.

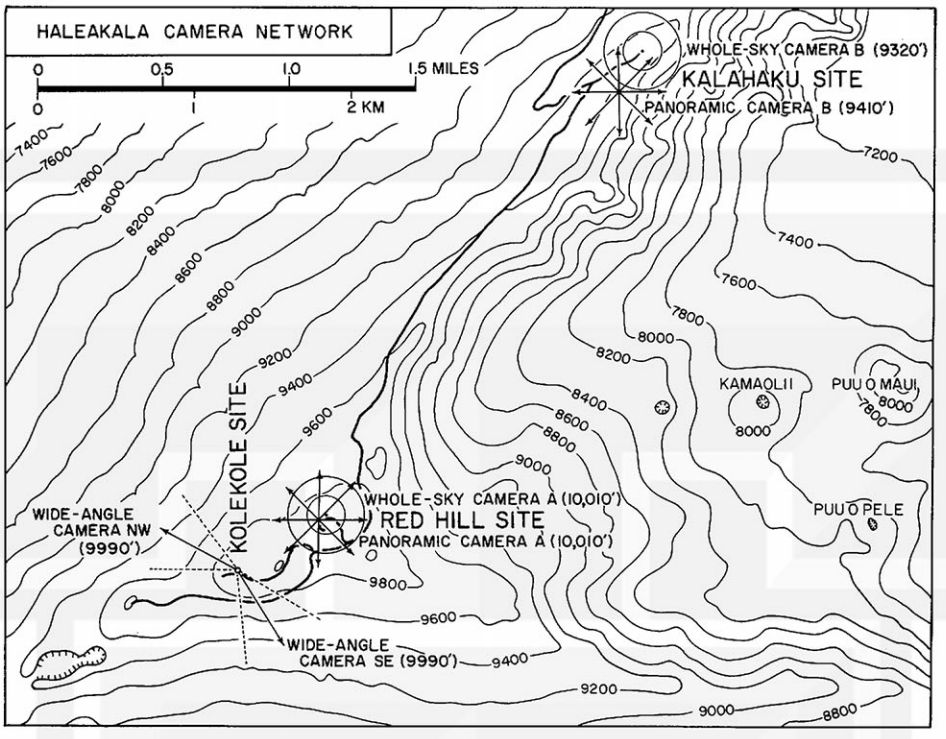

Fig. 1. The Haleakala camera network of March-April 1967. Two wide angle time lapse 16-mm movie cameras were operated at the Kolekole site (9990 ft); one to monitor clouds in the direction of the island of Hawaii and the other in the direction of Lanai. A stereo-pair of whole-sky and panoramic cameras were operated at the Red Hill site (10,010 ft) and at the Kolahaku site (9320-9410 ft), separated by a distance of 3.6 km, on the north rim of Haleakala on Maui.

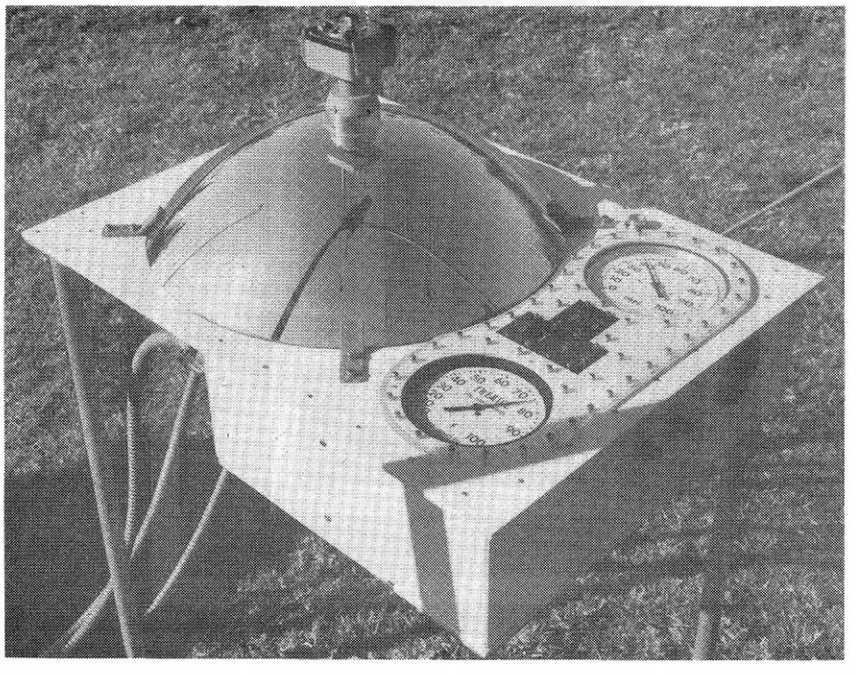

Fig. 2. A close-up of the parabolic mirror and data table of the Model A-20-EW whole sky camera system. Air temperature and relative humidity are indicated on the dials on the right hand side of the table. Rainfall amount in hundredths on an inch and wind-run in sixtieths of a statute mile are indicated on the counters. Time is indicated on the face of the Accutron clock mounted in the center of the mirror.

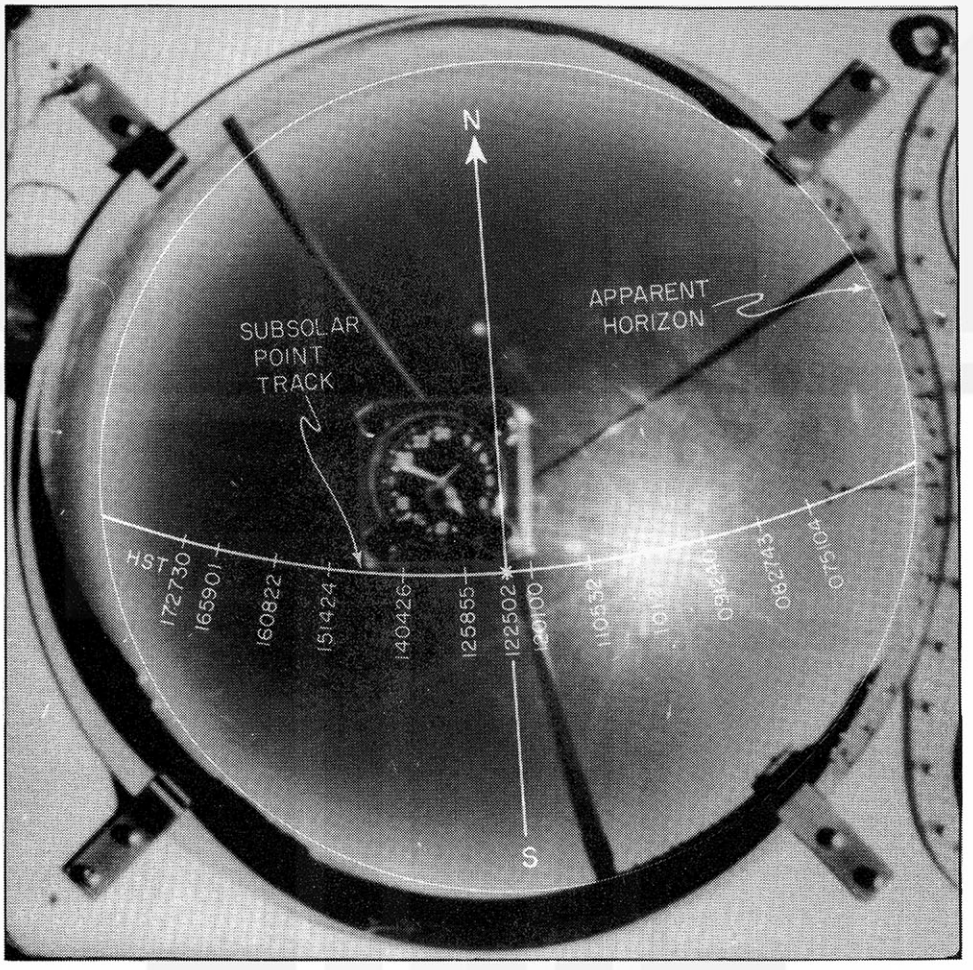

Fig. 3. Whole-sky picture with sun's image (subsolar point) and its path during the day on 14 March 1967. The whole-sky camera was located at the Red Hill site (Fig. 1) at 20° 42' 50" N, 156° 15' 23" W. Subsolar point locations at several times during the day are indicated along its path. Zero azimuth (N) intersects solar subpoint track at local noontime.

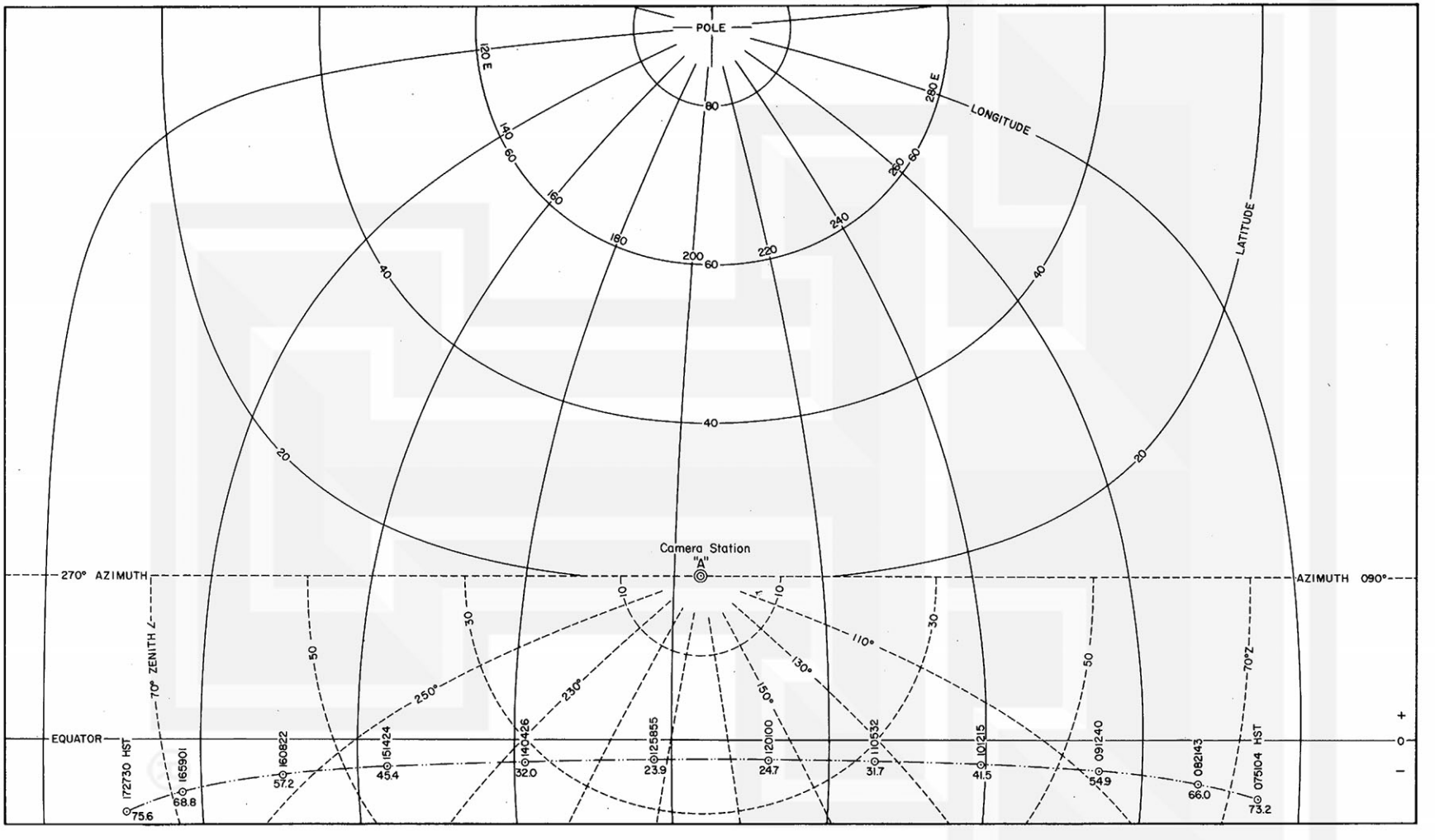

Fig. 4. Section of transverse equidistant cylindrical projection chart (TEC) (Solid lines) with the 12 subsolar points (Fig. 3) plotted at their computed geodetic latitude and longitude. Section of TEC overlay (dashed lines) showing selected latitude circles and meridians as zenith angles and azimuth, respectively.

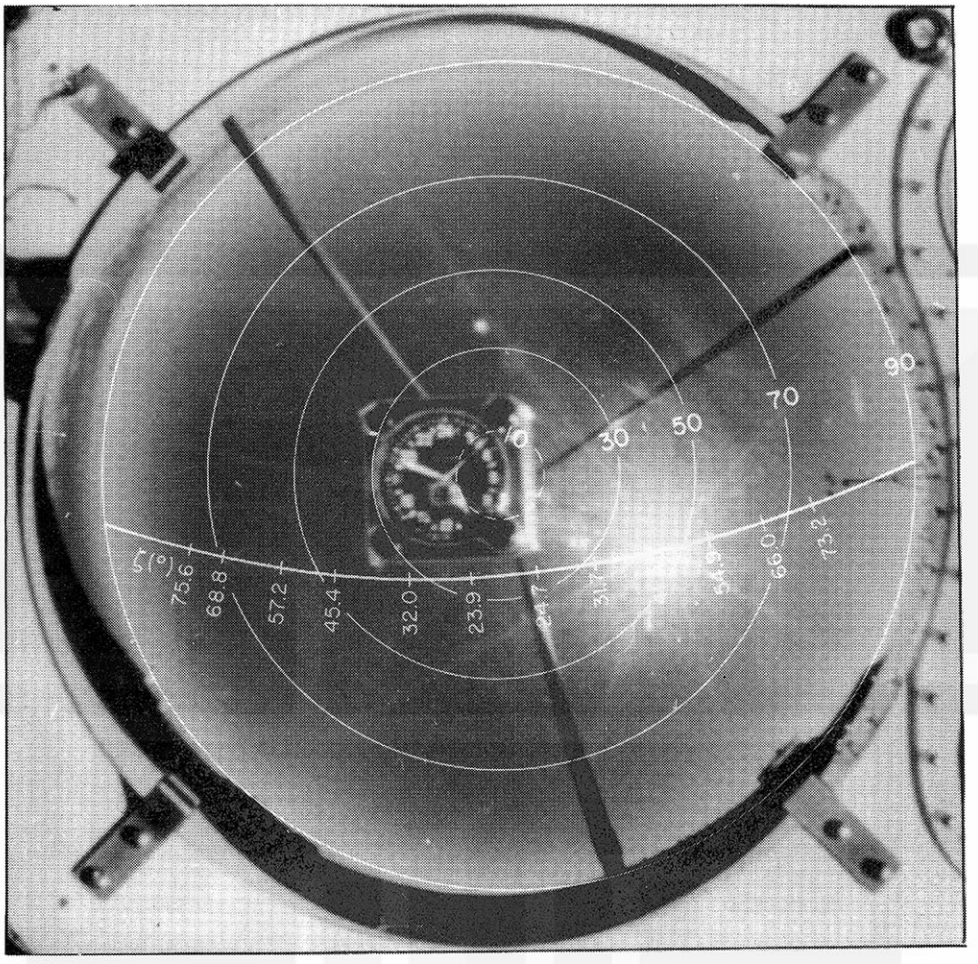

Fig. 5. Whole-sky picture with subsolar point track and computed solar zenith angles indicated along the track. Concentric circles represent zenith angles with the 90 degree circle indicating apparent horizon.

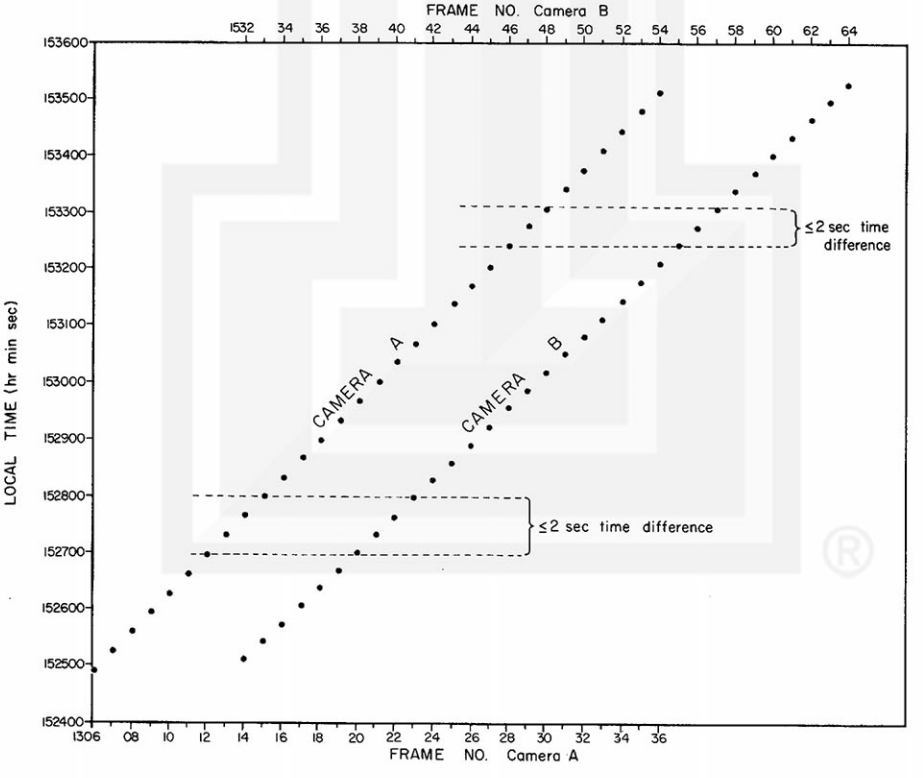

Fig. 6. Plot of frame number vs. picture time for the two whole-sky cameras. From this graph pairs of near synchronous pictures can be chosen.

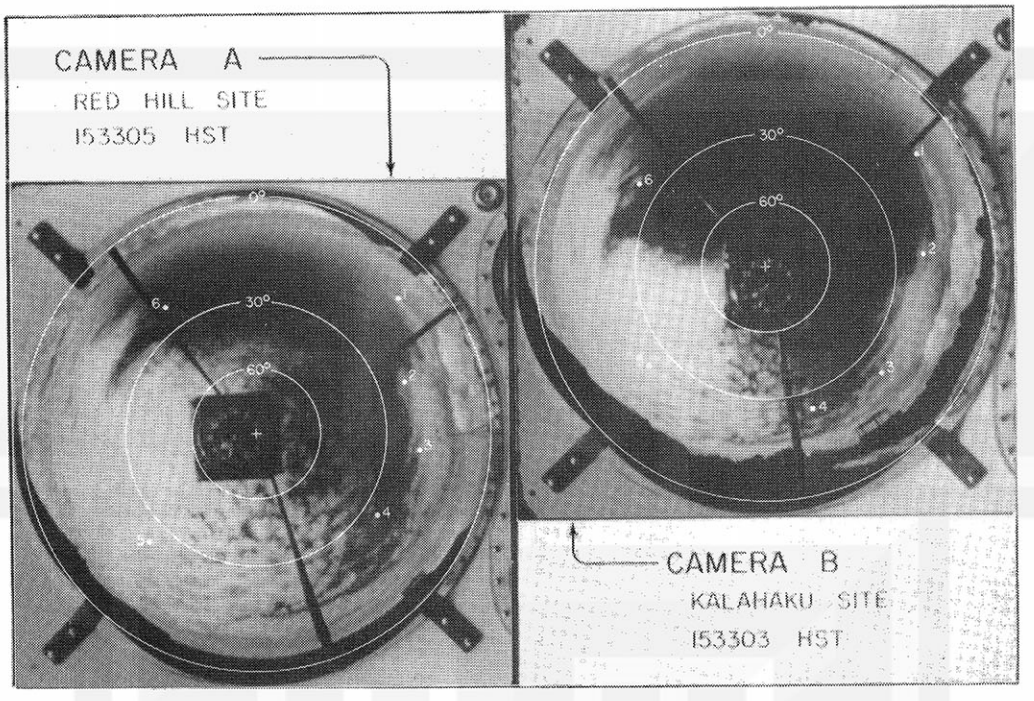

Fig. 7. An example of a stereo-pair of whole-sky pictures taken within two seconds of each other on 15 March 1967. The values on the concentric circles denote the elevation angles. Selected cloud elements for velocity and height computations are identified by numbers 1 through 6.

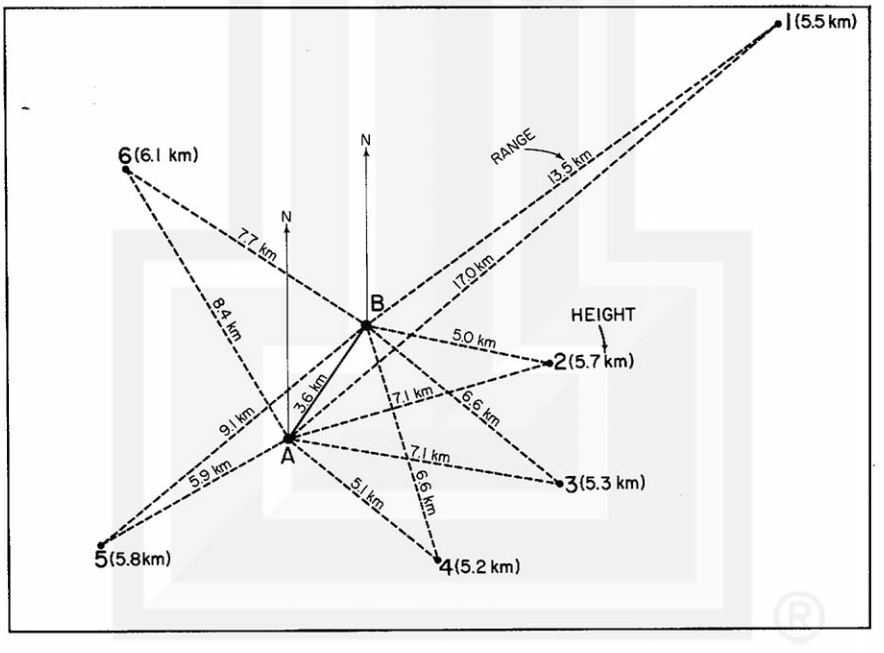

Fig. 8. An example of the plan-position determination by using the pair of pictures shown in Fig. 7. The baseline distance is 3.6 km. The height given in parenthesis denotes the mean cloud height (MSL) computed from the range and elevation angles from sites A and B.

MESOMETEOROLOGY PROJECT - - - RESEARCH PAPERS

(Continued from front cover)

42.* A Study of Factors Contributing to Dissipation of Energy in a Developing Cumulonimbus - Rodger A. Brown and Tetsuya Fujita

43. A Program for Computer Gridding of Satellite Photographs for Mesoscale Research - William D. Bonner

44. Comparison of Grassland Surface Temperatures Measured by TIROS VII and Airborne Radiometers under Clear Sky and Cirriform Cloud Conditions - Ronald M. Reap

45. Death Valley Temperature Analysis Utilizing Nimbus I Infrared Data and Ground-Based Measurements - Ronald M. Reap and Tetsuya Fujita

46. On the "Thunderstorm-High Controversy" - Rodger A. Brown

47. Application of Precise Fujita Method on Nimbus I Photo Gridding - Lt. Cmd. Ruben Nasta

48. A Proposed Method of Estimating Cloud-top Temperature, Cloud Cover, and Emissivity and Whiteness of Clouds from Short- and Long-wave Radiation Data Obtained by TIROS Scanning Radiometers - T. Fujita and H. Grandoso

49. Aerial Survey of the Palm Sunday Tornadoes of April 11, 1965 - Tetsuya Fujita

50. Early Stage of Tornado Development as Revealed by Satellite Photographs - Tetsuya Fujita

51. Features and Motions of Radar Echoes on Palm Sunday, 1965 - D. L. Bradbury and Tetsuya Fujita

52. Stability and Differential Advection Associated with Tornado Development - Tetsuya Fujita and Dorothy L. Bradbury

53. Estimated Wind Speeds of the Palm Sunday Tornadoes - Tetsuya Fujita

54. On the Determination of Exchange Coefficients: Part II - Rotating and Nonrotating Convective Currents - Rodger A. Brown

55. Satellite Meteorological Study of Evaporation and Cloud Formation over the Western Pacific under the Influence of the Winter Monsoon - K. Tsuchiya and T. Fujita

56. A Proposed Mechanism of Snowstorm Mesojet over Japan under the Influence of the Winter Monsoon - T. Fujita and K. Tsuchiya

57. Some Effects of Lake Michigan upon Squall Lines and Summertime Convection - Walter A. Lyons

58. Angular Dependence of Reflection from Stratiform Clouds as Measured by TIROS IV Scanning Radiometers - A. Rabbe

59. Use of Wet-beam Doppler Winds in the Determination of the Vertical Velocity of Raindrops inside Hurricane Rainbands - T. Fujita, P. Black and A. Loesch

60. A Model of Typhoons Accompanied by Inner and Outer Rainbands - Tetsuya Fujita, Tatsuo Izawa, Kazuo Watanabe, and Ichiro Imai

MESOMETEOROLOGY PROJECT - - - RESEARCH PAPERS

(Continued from inside back cover)

61. Three-Dimensional Growth Characteristics of an Orographic Thunderstorm System - Rodger A. Brown.

62. Split of a Thunderstorm into Anticyclonic and Cyclonic Storms and their Motion as Determined from Numerical Model Experiments - Tetsuya Fujita and Hector Grandoso.

63. Preliminary Investigation of Peripheral Subsidence Associated with Hurricane Outflow - Ronald M. Reap.

64. The Time Change of Cloud Features in Hurricane Anna, 1961, from the Easterly Wave Stage to Hurricane Dissipation - James E. Arnold.

65. Easterly Wave Activity over Africa and in the Atlantic with a Note on the Inter-tropical Convergence Zone during Early July 1961 - James E. Arnold.

66. Mesoscale Motions in Oceanic Stratus as Revealed by Satellite Data - Walter A. Lyons and Tetsuya Fujita.

67. Mesoscale Aspects of Orographic Influences on Flow and Precipitation Patterns - Tetsuya Fujita.

68. A Mesometeorological Study of a Subtropical Mesocyclone - Hidetoshi Arakawa, Kazuo Watanabe, Kiyoshi Tsuchiya, and Tetsuya Fujita.

69. Estimation of Tornado Wind Speed from Characteristic Ground Marks - Tetsuya Fujita, Dorothy L. Bradbury, and Peter G. Black.